ISSN 0023-1584, Kinetics and Catalysis, 2011, Vol. 52, No. 2, pp. 258–272. © Pleiades Publishing, Ltd., 2011.
Original Russian Text © A.V. Chistyakov, M.V. Tsodikov, V.Yu. Murzin, F.A. Yandieva, Ya.V. Zubavichus, N.Yu. Kozitsyna, A.E. Gekhman, V.V. Kriventsov, I.I. Moiseev, 2011, published in Kinetika i Kataliz, 2011, Vol. 52, No. 2, pp. 266–281.

Cocatalytic Effect of Palladium and Zinc in the Condensation of Alcohol Carbon Backbones into Hydrocarbons

A. V. Chistyakov[a], M. V. Tsodikov[a], V. Yu. Murzin[a], F. A. Yandieva[a], Ya. V. Zubavichus[b], N. Yu. Kozitsyna[c], A. E. Gekhman[c], V. V. Kriventsov[d], and I. I. Moiseev[a]

[a] *Topchiev Institute of Petrochemical Synthesis, Russian Academy of Sciences, Moscow, 119991 Russia*
[b] *Kurchatov Institute Russian Research Center, Moscow, 123182 Russia*
[c] *Kurnakov Institute of General and Inorganic Chemistry, Russian Academy of Sciences, Moscow, 119991 Russia*
[d] *Boreskov Institute of Catalysis, Siberian Branch, Russian Academy of Sciences, Novosibirsk, 630090 Russia*
e-mail: chistyakov@ips.ac.ru

Received July 2, 2010

Abstract—The results of the direct conversion of ethanol and its mixture with glycerol into a $C_4 - C_{10+}$ alkane and olefin fraction in the presence of Pd-, Zn-, and Pd–Zn-containing catalysts, which were prepared by supporting homo- and heterometallic acetate complexes onto the surface of γ-Al_2O_3, are reported. It was found that, in the presence of mono- and bicomponent Pd–ZnO (Pd; ZnO)/γ-Al_2O_3 systems, selectivity in the formation of alkanes, olefins, or their mixtures in the target fraction can be controlled as a result of the cocatalytic effect of active components that are responsible for the catalyst activity in condensation and hydrogenation reactions. The structures of the active components were studied and the genesis of the catalytic systems was characterized using XAFS, XPS, and XRD analysis. It was found that the addition of glycerol considerably increased the yield of the target hydrocarbon fraction.

DOI: 10.1134/S0023158411020030

INTRODUCTION

Alcohol conversion with the predominant formation of alkanes containing at least a doubled number of carbon atoms in their skeletons, as compared with that in the parent alcohol, is referred to as a reductive dehydration reaction [1]. This reaction has been studied previously on catalytic systems having a pronounced hydrogenating function, such as polymetallic intermetallides, molten iron, and a commercial alumina–platinum catalyst (AP-64) [1–3]:

$$m\mathrm{C_2H_5OH} + 2[\mathrm{H}] \longrightarrow \mathrm{C}_n\mathrm{H}_{2n+2} + m\mathrm{H_2O}. \quad \text{(I)}$$

Note that the conversion of alcohols in the presence of nanosized metal oxide catalysts occurs with the formation of olefins in two alternative directions: the condensation and cross-condensation of the carbon skeletons of various alcohols [4–6] in accordance with the general reaction scheme

$$2\mathrm{RHOH} \longrightarrow [\mathrm{R{=}R}] + 2\mathrm{H_2O}, \quad \text{(II)}$$

$$\mathrm{R^1HOH} + \mathrm{R^2HOH} \longrightarrow [\mathrm{R^1 = R^2}] + 2\mathrm{H_2O}. \quad \text{(III)}$$

These results suggest multivariant reaction paths in the conversion of alcohols depending on the nature and structure of active centers.

To control selectivity and activity, heterogeneous catalysts containing bimetallic active components supported onto a substrate, which are prepared based on heterometallic metal complex compounds, have been widely used in recent years [7–10]. However, the nature of mutual effects of active components with each other and the support surface has been poorly studied. The interaction mechanism mainly depends on the distance between active components distributed over the support surface and on the charge state of these components, which depends on the thermal pretreatment procedure.

In this work, catalysts based on the acetate complexes of Pd, which were responsible for the occurrence of reaction path (I), and a typical Zn/Al_2O_3 acid catalyst for oxygenate condensation reactions, which was responsible for reaction paths (II) and (III), were chosen as test materials.

The use of heterometallic acetate complexes as precursors, in which palladium and zinc atoms approach each other within a single structure, is the most interesting problem. These complexes result in the formation of heterometallic active centers on the surface of γ-Al_2O_3, as described previously [9, 10], to affect activity and selectivity in the reaction of ethanol conversion into aliphatic hydrocarbons (the reductive dehydration of ethanol).

The aim of this work was to study the reaction of ethanol conversion into hydrocarbons on these catalysts and to characterize the structure and catalytic activity of systems prepared from mono- and bimetallic acetate complexes. In addition, it was important to study the effect of the pretreatment procedure and the

amounts of active components supported onto the surface of γ-Al_2O_3 on genesis and catalytic properties.

EXPERIMENTAL

Commercial γ-Al_2O_3 with the following characteristics was used as the support: spherical granules with a sphere size of 2.0–3.0 mm; specific surface area, no less than 190 m^2/g (OST [Branch Standard] 153-39.2-022-2002); pore volume, 0.65 cm^3/g (OST 153-39.2-023-2002); iron impurity content, no more than 0.14 wt %; sodium impurity content, no more than 0.1 wt %; sorption capacity for insulating gas, no more than 10 g/kg; and sorption capacity for hydrogen (deuterium) fluoride, no less than 7 g/kg.

The acetate complexes $Zn(OAc)_2 \cdot 2H_2O$, $Pd_3(OAc)_6$, and $Pd(\mu\text{-}OOCMe)_4Zn(OH_2)$ were used to prepare mono- and bimetallic catalytic systems [11]. The palladium atom in a bimetallic complex is strongly bound to the zinc atom by four acetate bridges, and the metal–metal distance is 2.57 Å, which is close to the sum of the van der Waals radii of palladium and zinc atoms (2.53 Å). Figure 1 shows the structure of the binuclear acetate complex of palladium with zinc.

The complexes were supported onto γ-Al_2O_3 from solutions in methanol by impregnation in accordance with the following procedure: aluminum oxide granules calcined at 350°C were placed in a hermetically sealed vessel and thoroughly purged with argon. In flowing argon, a calculated amount of an acetate complex solution was measured with consideration for incipient wetness impregnation and added to the aluminum oxide; the granules were stirred at regular intervals. After 2 h, the granules were dried in air for 15 h and then in a vacuum oven at 80°C for 5 h; thereafter, they were calcined in a muffle furnace (Ar) at 500°C for 5 h.

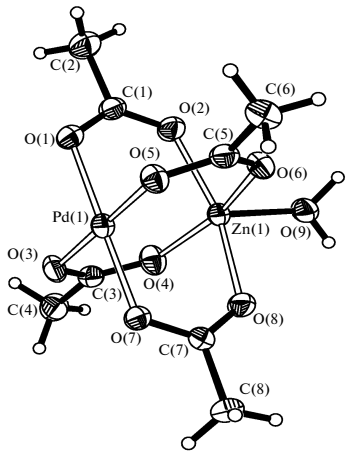

Fig. 1. Structure of the binuclear acetate complex of palladium with zinc $Pd(\mu\text{-}OOCMe)_4Zn(OH_2)$.

The metal-containing catalytic systems thus prepared were thermally treated under various conditions before catalytic tests. The concentrations of metals in the synthesized catalyst samples were determined by inductively coupled plasma atomic emission spectrometry (ICP AES). Table 1 summarizes the used metal complex precursors and pretreatment procedures.

Ethanol of analytical grade was used without preliminary purification. The catalytic experiments were performed in a laboratory flow-circulation system with a fixed catalyst bed in Ar under previously found optimum conditions for ethanol conversion: temperature, 350°C; pressure, 50 atm; ethanol supply rate, 0.6 h^{-1}; and gas circulation rate, 50 cm^3/min [5, 6].

Ethanol was supplied to an evaporator using a high-precision plunger feeder (HPP 5001), and vapor from the evaporator arrived at a reactor. The reaction products arrived at a cooled gas–liquid separator, after

Table 1. Catalytic systems and preparation procedures

No.	Active components (concentration, wt %)	Starting complex for supporting onto γ-Al_2O_3	Pretreatment procedure	
			stage 1	stage 2
I	Pd (1.07)	$Pd_3(OAc)_6$	Calcination in flowing argon; $T = 500$°C, 5 h	10 h at 450°C in flowing hydrogen; 10 l/h
II	Zn (1.03)	$Zn(OAc)_2 \cdot 2H_2O$	″	″
III	Pd-Zn (0.72 : 0.43)	$Pd(\mu\text{-}OOCMe)_4Zn(OH_2)$	″	″
IIIa*	Pd-Zn (2.40 : 1.43)	″	″	″
IV	Pd+Zn (0.70 : 0.41)	$Pd_3(OAc)_6$; $Zn(OAc)_2 \cdot 2H_2O$; step-by-step supporting	″	″
V	Pd/Zn (0.72 : 0.43)	$Pd(\mu\text{-}OOCMe)_4Zn(OH_2)$	Reduction in flowing hydrogen; 5 K/min to 450°C; 8 h at 450°C in flowing hydrogen	″

* Catalyst **IIIa** with a triple concentration of active components was prepared in accordance with a procedure identical to that for catalyst **III**.

which the condensed liquid fraction was collected in a receiver. After the separator, a mixture of argon with uncondensed reaction products was returned to the reaction volume of the system using a circulation pump.

The gaseous reaction products were analyzed by on-line gas chromatography. The C_1–C_5 hydrocarbon gases were determined on a Kristall-4000 chromatograph (FID; He, 70 cm^3/min; 120°C; $P = 0.65$ MPa; HP-PLOT/Al_2O_3 column, 50 m × 0.32 mm).

The analysis for CO, CO_2, and H_2 was performed on a Kristall-4000 chromatograph (TCD; Ar (high purity); SKT column, 150 × 0.4 cm; 130°C; 30 ml/min). Low concentrations of CO (<0.4 vol %) were determined using a Riken Keiki gas analyzer with an IR cell (model RI-550A).

The liquid organic reaction products in aqueous and organic phases were identified by gas chromatography–mass spectrometry (GC–MS) on MSD 6973 (Agilent) and Automass-150 (Delsi Nermag) instruments; EI = 70 eV; sample volume, 1 μl; HP-5MS column, 0.32 × 500 cm, $D_f = 0.52$ mm; 50°C (5 min); 10 K/min; 270°C; $T_{inj} = 250$°C; constant flow rate of 1 ml/min; split ratio, 1 : 100–200; CPSil-5, 0.15 × 250 cm, $D_f = 1.2$ mm; 50°C (8 min); 10 K/min; 270°C; $T_{inj} = 250$°C; $P_{inj} = 2.2$ bar; split ratio, 1 : 300. Quantitatively, the concentrations of organic substances were determined by GLC on a Varian 3600 instrument; SE-30 Chromtec column, 0.25 × 250 cm, $D_f = 0.3$ mm; 50°C (5 min); 10 K/min; 280°C; $T_{inj} = 250$°C; $P_{inj} = 1$ bar; split ratio, 1 : 200; FID; trifluoromethylbenzene was used as an internal standard for an organic layer, and internal normalization was used for an aqueous layer. The ethanol content of the aqueous phase was determined by GC–MS from a ratio between the integrated signals of ethanol and water using the absolute calibration technique.

The charge states of metal-containing active catalyst components were studied by XPS.

The photoelectron spectra were measured at room temperature on an XSAM-800 spectrometer from Kratos (United Kingdom) using nonmonochromatic MgK_α radiation whose power was no higher than 90 W. The spectra were measured under conditions of a constant relative energy resolution with a step of 0.1 eV. The measurements were performed at a pressure of ~5×10^{-8} Pa in the analytical chamber. The analyzed spectra were approximated by a Gaussian profile or a sum of these profiles, and the background due to secondary electrons and photoelectrons that underwent energy losses was approximated by a straight line. The energy scale of the spectrometer was calibrated in accordance with a standard procedure using the following binding energies: Cu $2p_{3/2}$, 932.7 eV; Ag $3d_{5/2}$, 368.3 eV; and Au $4f_{7/2}$, 84.0 eV. Quantitative analysis was performed based on element sensitivity factors from the software provided by the manufacturer. The samples were fixed with a double-sided Scotch tape. The surface charging for support spectra was taken into account using the C 1*s* spectrum in accordance with a traditional procedure. The C–CH state was recognized in the spectrum, and an energy of 285.0 eV was ascribed to it. The calibration of the spectra of other samples was performed using the Al 2*p* peak in the spectrum of the support. The spectra were measured at room temperature.

The charge states and local structures of metal-containing active components were studied by XAFS spectroscopy at the Structural Materials Science station of the Kurchatov Center of Synchrotron Radiation and Nanotechnology [8]. The *K*-edge absorption spectra of zinc and palladium were measured in the transmission mode using two ionization chambers filled with the corresponding mixtures of nitrogen and argon to provide 20 and 80% absorption for I_0 and I_t, respectively. For the monochromatization of a synchrotron radiation beam, monoblock cut Si(111) and Si(220) monochromators were used (for the *K* edges of Zn and Pd, respectively). The catalyst powder was pressed as a pellet 1.5 mm in thickness before the measurements. Programs from the IFEFFIT package [12] were used for the processing of spectra, and photoelectron scattering phases and amplitudes used for the refinement of local structure parameters were calculated using the FEFF program [13, 14]. The range of electron wave numbers (k) in the model refinement procedure was 3.0–13.0 $Å^{-1}$.

The diffraction patterns of catalysts were also measured with the use of synchrotron radiation at the Structural Materials Science station of the Kurchatov Center of Synchrotron Radiation and Nanotechnology. The diffraction patterns were measured in the transmission geometry (Debye–Scherrer) using Fuji-Film photosensitive imaging plates as a detector. The wavelength was $\lambda = 0.69$ Å, and the exposure time was 15 min.

RESULTS AND DISCUSSION

Catalytic Activity and Selectivity of Pd,Zn-Containing Systems in the Reductive Dehydration of Ethanol

On the test catalysts, ethanol is converted into C_1–C_{11} alkanes and olefin hydrocarbons, carbon oxides, liquid oxygenates, and water. Table 2 summarizes the balance of the yields of reaction products on a carbon basis (mol %) in the presence of mono- and bimetallic catalysts.

It was found that the maximum yield of the target fraction of C_3–C_{10} aliphatic hydrocarbons (~50 wt %) was reached upon catalysis using a Pd–Zn-containing system prepared by supporting the heterometallic acetate complex Pd(μ-OOCMe)$_4$Zn(OH$_2$) on Al_2O_3 (**III**) (Fig. 2). With the use of monometallic systems containing Pd (**I**) or Zn (**II**) with active component concentrations equivalent to the concentration in the heterometallic system, a decrease in the yield of the target fraction by 25 or 10 wt %, respectively, was observed.

Table 2. Balance on carbon in the conversion of ethanol in the presence of catalysts **I–III***

Pd (catalyst **I**)			Zn (catalyst **II**)			Pd–Zn (catalyst **III**)		
C supplied, %	C obtained, %		C supplied, %	C obtained, %		C supplied, %	C obtained, %	
100.00	C1	11.79	100.00	C1	0.28	100.00	C1	2.62
	C2	20.78		C2	24.10		C2	21.77
	C3	12.06		C3	3.48		C3	2.22
	C4	19.31		C4	32.14		C4	28.46
	C5	0.86		C5	3.12		C5	2.78
	C6	6.10		C6	7.96		C6	13.68
	C7	1.26		C7	2.25		C7	2.19
	C8	2.03		C8	1.52		C8	3.74
	C9	0.20		C9	0.14		C9	0
	C10	0.48		C10	0		C10	0
	C11	0.12		C11	0		C11	0
	Oxygenates	6.79		Oxygenates	23.75		Oxygenates	17.54
	Aromatics	1.60		Aromatics	1.27		Aromatics	0.97
	CO	14.23		CO	0		CO	2.99
	CO_2	2.38		CO_2	0		CO_2	1.04
	Total	100.00		Total	100.00		Total	100.00

* The data are given in mol %.

Note that alkanes were predominant among the products of ethanol conversion on the Pd-containing catalyst, whereas the target fraction contained 70 wt % olefins and only 30 wt % alkanes on the Zn-containing catalyst. A more detailed analysis of the reaction products (Table 3) indicated that, in the case of the Zn-containing system, a considerable yield of ethylene (126.61 mmol) and the complete absence of carbon monoxide and carbon dioxide were observed in contrast to the Pd-containing system, in which the yields of carbon oxides were 193.13 and 32.35 mmol, respectively, and ethylene was absent (Table 3).

These results suggest radically different reaction paths in the conversion of ethanol on Pd- and Zn-containing systems. Figure 3 shows the distribution of hydrocarbons in the target fraction for these catalysts (**I, II**).

Thus, the composition of products prepared on the palladium-containing system was close to the composition prepared in the presence of a commercial alumina–platinum catalyst [15]. This fact suggests the identity of reaction paths in ethanol conversion on the above systems. Previously, it was found that a possible reaction path in ethanol conversion into linear alkanes with even numbers of carbon atoms is the incorporation of ethylene, which is formed from ethanol and circulates in a gas mixture through a catalyst bed, into carbon chain growth [15].

We can also hypothesize that the formation of target products (C_{3+} alkanes) on the palladium-containing catalyst results from the participation of surface ethylene, which is formed in the reaction of ethylene dehydration, in carbon chain growth followed by hydrogenation at palladium-containing sites, as shown in the following reaction scheme:

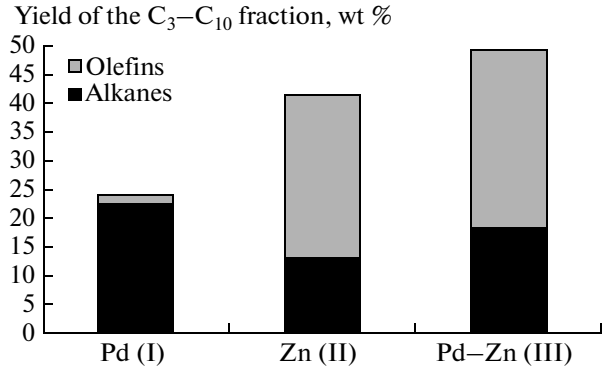

Fig. 2. Yields of C_3–C_{10} alkane and olefin fractions obtained from ethanol in the presence of mono- and bimetallic catalysts.

Table 3. Yields (mmol) of the conversion products of 700 mmol of ethanol on Pd- and Zn-containing systems

Products	Pd (**I**)			Zn (**II**)			Pd–Zn (**III**)		
	alkanes	olefins	others	alkanes	olefins	others	alkanes	olefins	others
Aliphatic hydrocarbons									
C_1	160.01	–	–	4.00	–	–	36.34	–	–
C_2	141.01	0	–	43.45	126.61	–	92.68	58.02	–
C_3–C_{10}	99.40	6.68	–	26.18	59.21	–	51.09	78.91	–
Other products									
Oxygenates	–	–	11.38	–	–	28.97	–	–	28.39
Aromatics	–	–	2.01	–	–	1.32	–	–	1.58
CO	–	–	193.13	–	–	0	–	–	41.39
CO_2	–	–	32.35	–	–	0	–	–	14.34
H_2	–	–	18.07	–	–	5.60	–	–	0.50

$$H_3C{-}CH_2{-}OH \xrightarrow{-H_2O} H_2C{=}CH_2 \xrightarrow{+C_2H_4} \ldots \xrightarrow{+C_2H_4} C_nH_{2n} \xrightarrow{+H_2} C_nH_{2n+2}. \quad \text{(IV)}$$

As was found previously [5], it is most likely that hydrogen, which is required for the formation of alkanes by reaction (I), and carbon monoxide result from the reaction of ethanol dehydrogenation followed by the decarbonylation of acetaldehyde:

$$H_3C{-}CH_2{-}OH \xrightarrow{-H_2} H_3C{-}C\begin{matrix}=O\\ \diagdown H\end{matrix} \longrightarrow CH_4 + CO. \quad \text{(V)}$$

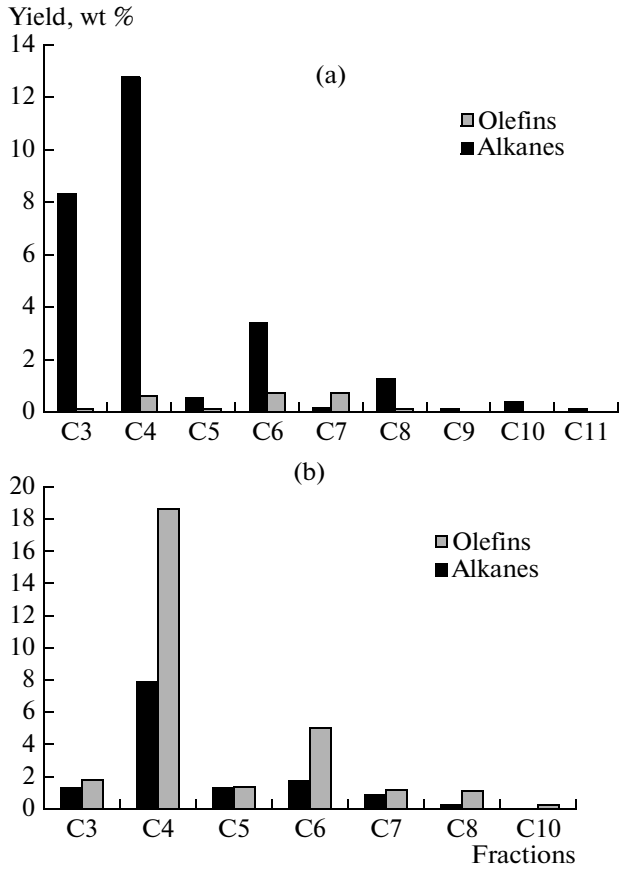

Fig. 3. Fractional composition of C_3–C_{10} hydrocarbons obtained from ethanol in the presence of catalysts (a) **I** and (b) **II**.

The predominance of linear alkanes, whose concentration was higher than 90 wt %, in the reaction products suggests the above reaction path. Note that alkanes with even numbers of carbon atoms were predominant (Fig. 3a, Table 4). Alkanes with odd numbers of carbon atoms, whose concentration was much lower (see Fig. 3a), can result from the decarbonylation reactions of acetaldehyde homologs. The water gas shift reaction can occur simultaneously to cause the formation of carbon dioxide:

$$CO + H_2O \longrightarrow CO_2 + H_2.$$

This was indirectly supported by the equivalent yields of carbon oxides and alkanes with odd numbers of carbon atoms: 204.29 and 225.48 mmol, respectively.

Note that the high hydrogenating activity of reduced palladium negatively affects the oligomerization of olefins because of the occurrence of a competing reaction of ethylene hydrogenation, which results in the termination of carbon chain growth. The similar yields of C_{3+} alkanes (27 wt %) and ethane (20 wt %) suggest similar rates of the competing reactions. The process selectivity also considerably decreases because of the formation of methane and carbon oxides, whose total yield was close to 35 wt %.

With the use of the zinc-containing system, the most likely reaction mechanism seems involve the dehydrogenation of ethanol with the formation of acetaldehyde

followed by the aldol condensation of acetaldehyde to form monomethyl-substituted carbon chains and the reduction of the resulting oxygenates [16]:

$$C_2H_5OH \xrightarrow{-H_2} CH_3COH \xrightarrow{+(n-3)AcH} HOC_nH_{2n}COH \xrightarrow{+H_2} CH_3CH_2CH(CH_3)C_mH_{2m}, \quad \text{(VI)}$$

where $n \le 11$ and $m = n - 3$.

The low hydrogenating activity of the zinc catalyst does not provide for the occurrence of reductive dehydration to selectively form alkanes (reaction scheme (VI)). However, the composition of olefin products is consistent with this reaction path (Fig. 3b). It was found that the concentration of hydrocarbons with branched structures was 50–60% (3-methyl-substituted derivatives were predominant) after the hydrogenation of a C_{3+} olefin fraction in the presence of the well-known Ni/Al_2O_3 catalyst for this reaction.

As found previously, a number of oxygenates such as diethyl ether and acetaldehyde were also converted into aliphatic hydrocarbons in the presence of a commercial alumina–platinum catalyst (AP-64) as the contact time was increased [15]. In this context, the oxygenates, which are produced in a sufficiently high yield, can be considered as raw materials for recycling in order to obtain an additional amount of hydrocarbons.

Note that the yield of ethylene was high (126.61 mol). As noted above, ethylene may participate in the formation of linear aliphatic hydrocarbons upon catalysis by the palladium system. However, it is likely that the accumulation of ethylene in reaction products was due to a small contribution of conversion in accordance with reaction scheme (IV) in the presence of system **II**.

Thus, the hypothesis of the occurrence of both of the reaction paths in the presence of the Pd–Zn catalyst based on a heterometallic precursor seems reasonable.

As can be seen in Table 3 and Fig. 2, upon the conversion of ethanol on palladium–zinc system **III**, the liquid products contained approximately the same amounts of alkanes and alkenes.

This fact suggests an additive catalytic effect of palladium and zinc in the reactions of ethanol conversion. It is most likely that this effect was due to the complementarity of ethanol conversions in reactions (I) and (II). As can be seen in Table 3, small amounts of ethylene and carbon oxides were present in the reaction products; this fact indicates that the reaction simultaneously occurred via reaction paths (IV)–(VI).

Thus, the experimental results demonstrate that the process that occurs in the presence of palladium–zinc catalytic system **III**, which was prepared from a heterometallic precursor, is most selective for a fraction of aliphatic hydrocarbons. In this case, a maximum yield of aliphatic hydrocarbons is higher than 80% on a theoretical basis.

Table 4. Ratios between the yields of the nearest hydrocarbon homologs formed upon ethanol conversion on palladium-containing catalyst **I**

Homologs	Yield ratio
C_4/C_3	1.52
C_6/C_5	6.53
C_8/C_7	9.75
C_{10}/C_9	2.38

Table 5. Yields (mmol) of the conversion products of 700 mmol of ethanol in the presence of catalytic system **IIIa**

Products	Alkanes	Olefins	Others
Hydrocarbons			
C_1	97.50	–	–
C_2	77.43	0.17	–
C_3–C_9	47.54	1.48	–
Other products			
Oxygenates	–	–	26.17
Aromatics	–	–	0
CO	–	–	289.30
CO_2	–	–	53.11
H_2	–	–	123.10

To intensify the process of ethanol conversion, we performed a reaction with the use of catalyst **IIIa**, in which the concentration of Pd–Zn active components was higher than that in the above example by a factor of 3.

In Table 5, it can be seen that the yields of alkanes, carbon monoxide, methane, and hydrogen noticeably increased in the presence of catalyst **IIIa** (as compared with catalyst **III**). The yield of the target fraction of aliphatic hydrocarbons decreased by a factor of >3; olefins were also almost completely absent from the reaction products. This behavior of the catalytic system suggests that an increase in the amount of palladium-containing centers resulted in the predominance of reaction path (IV) and the suppression of activity in the process of carbon skeleton condensation via reaction path (VI).

In this context, we can hypothesize that, as the amount of active components was increased, palladium-containing centers became predominant in ethanol conversion and the role of zinc-containing centers decreased.

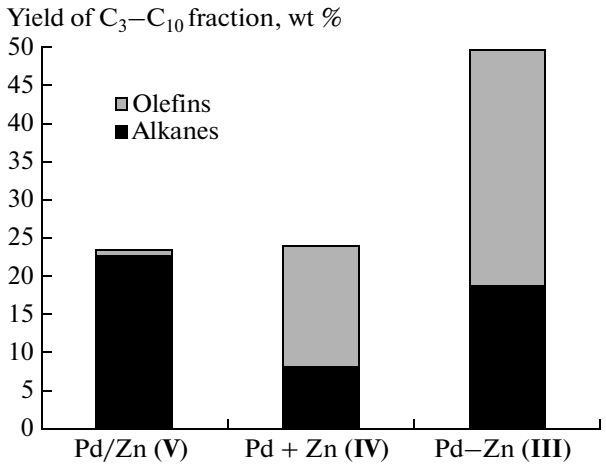

Fig. 4. Yields of the products of ethanol conversion in the presence of bimetallic catalysts prepared by various procedures.

We found that the catalyst pretreatment procedure and the nature of the metal complex precursors used exerted a considerable effect on process selectivity.

It is believed that, upon supporting active components from a heterometallic complex, these components were arranged on the support surface at distances close to the sum of the van der Waals atomic radii of the metals to provide the bifunctional character of these clusters [9]. This was demonstrated above using ethanol conversion as an example. To test this hypothesis, we prepared catalyst **IV** by the separate supporting of homometallic precursors $Zn(OAc)_2 \cdot 2H_2O$ and $Pd_3(OAc)_6$ onto the support.

As can be seen in Fig. 4 and Table 6, the yield (wt %) of the target fraction of hydrocarbons on this catalyst decreased by a factor of >2, and the yield of the ethane–ethylene fraction also increased by a factor of ~2. The yield of oxygenates remained at an approximately the same level as that in the case of a catalyst based on a heterometallic complex. Thus, on the catalyst in which active components are supported nonuniformly and separated by considerable distances, the effect of the cocatalytic reaction enhancement considerably decreased.

Previously, a procedure for the preparation of a Pd–Zn alloy by supporting the heterometallic complex $Pd(\mu\text{-}OOCMe)_4Zn(OH_2)$ followed by reduction in hydrogen has been developed [9, 10].

We used this procedure to prepare catalyst **V**. The tests of this catalyst in ethanol conversion demonstrated that the yield of the target fraction of C_3–C_{10} hydrocarbons was almost the same that the yield observed with the system containing only palladium (Fig. 4, Table 6). Alkanes dominated in the products of ethanol conversion, and ethylene was almost absent. Nevertheless, a decrease in the yields of carbon oxides and methane and a simultaneous increase in the yield of olefins suggest the occurrence of reaction paths typical of the zinc-containing system (Fig. 3, Table 2). It is likely that the formation of intermetallide clusters considerably intensified reaction paths (IV) and (V), which are characteristic of the palladium-containing system. However, a number of zinc atoms were distributed over the surface of $\gamma\text{-}Al_2O_3$.

To study the cross-condensation reaction of the carbon skeletons of different alcohols, we used glycerol as a coreactant for ethanol. We found that glycerol added to ethanol in an amount of no more than 30 wt % was an active coreactant in the formation of C_4–C_{10+} aliphatic hydrocarbons to considerably increase the yield of these hydrocarbons. The composition of reaction products essentially depends on the composition of palladium–zinc-containing systems.

Table 7 summarizes the results of the combined conversion of 70 wt % ethanol and 30 wt % glycerol on

Table 6. Yields (mmol) of the conversion products of 700 mmol of ethanol in the presence of Pd- and Zn-containing systems

Products	Pd + Zn (**IV**)			Pd/Zn (**V**)			Pd–Zn (**III**)		
	alkanes	olefins	others	alkanes	olefins	others	alkanes	olefins	others
Aliphatic hydrocarbons									
C_1	53.12	–	–	79.86	–	–	36.34	–	–
C_2	101.25	197.82	–	165.16	0.61	–	92.68	58.02	–
C_3–C_{10}	25.37	46.05	–	64.55	1.36	–	51.09	78.91	–
Other products									
Oxygenates	–	–	28.64	–	–	68.51	–	–	28.39
Aromatics	–	–	0.11	–	–	0	–	–	1.58
CO	–	–	56.33	–	–	85.15	–	–	41.39
CO_2	–	–	16.93	–	–	20.27	–	–	14.34
H_2	–	–	1.48	–	–	8.60	–	–	0.50

Table 7. Yields (wt %) of the conversion products of 70 wt % ethanol and 30 wt % glycerol on Pd- and Zn-containing systems

Products	Pd (**I**)			Zn (**II**)			Pd–Zn (**III**)		
	alkanes	olefins	others	alkanes	olefins	others	alkanes	olefins	others
Aliphatic hydrocarbons									
C_1	2.13	–	–	0.18	–	–	0.17	–	–
C_2–C_3	8.41	24.35	–	6.97	16.04	–	2.24	10.82	–
C_4–C_{10}	15.80	24.08	–	14.25	37.32	–	11.00	27.05	–
Other products									
Oxygenates	–	–	16.09	–	–	16.64	–	–	35.14
Aromatics	–	–	2.40	–	–	2.21	–	–	2.64
CO	–	–	7.08	–	–	2.42	–	–	5.16
CO_2	–	–	2.72	–	–	3.86	–	–	1.87
H_2	–	–	0.01	–	–	0.05	–	–	0.01

the palladium-containing system. Note that the addition of glycerol facilitated an increase in the total yield of hydrocarbons by ~10 wt % because of an increase in the yield of olefins. Among other distinctive features, note an increase in the yield of oxygenates from 5 wt % in ethanol conversion to 15 wt % in the combined reaction. The yield of carbon oxide and carbon dioxide decreased from >30 wt % and the yield of methane decreased from 12 wt % in the case of ethanol to 2 wt % in the conversion of the mixture of the alcohols.

It is most likely that this fact suggests the competitive chemisorption of ethanol and glycerol at catalytic active sites. Zinc-containing system **II** exhibited the highest activity in the cross-condensation reaction. In the presence of this system, the yield of the alkane–olefin fraction increased to 50 wt %. Data given in Table 7 indicate that the increase in the yield of the target hydrocarbon fraction was due to an increase in the yield of olefins; in this case, the yield of alkanes remained at the same level (12–15 wt %). The increase in the yield of unsaturated hydrocarbons can be explained by the fact that the glycerol molecule contains three hydroxyl groups and a triple amount of hydrogen is required for the saturation of C–C bonds upon its deoxygenation, as compared with ethanol. Note that the yield of propylene increased considerably and the yield of propane decreased. It is likely that the remaining 12% glycerol participated in the increase of the yield of hydrocarbons, mainly, the C_{5+} fraction, by reaction (III).

In the presence of heterometallic palladium–zinc-containing system **III**, the concentration of the alkane–alkene fraction decreased mainly as a result of an increase in the yield of oxygenates (Table 7).

Data given in Table 8 can be used to estimate the contribution of glycerol to the formation of one or another hydrocarbon. Table 8 summarizes the ratios of the yields of hydrocarbons prepared by the conversion of a mixture of 70% ethanol and 30% glycerol to the yields of hydrocarbons prepared by the conversion of only ethanol.

The above data indicate that, with the use of glycerol as a coreactant, the yield of the ethane–ethylene fraction decreased by a factor of 2, and the yield of C_5–C_7 hydrocarbons increased by a factor of 4; in the case of C_{10}, the yield increased by a factor of 6.

Thus, the composition of the catalytic system prepared based on aluminum oxide and acetate homo- and heterometallic complexes essentially affected the direction of C_2–C_3 alcohol conversion reaction into a fraction of C_4–C_{10} aliphatic hydrocarbons. It is evident that the found high sensitivity of the reaction was due to different structures of catalytically active complexes.

Table 8. Ratios between the yields of hydrocarbons obtained from ethanol (e) and a mixture of ethanol and glycerol (m)

Yield ratio	Pd (**I**)		Zn (**II**)	
	alkanes	olefins	alkanes	olefins
C_{1m}/C_{1e}	0.36	–	0.05	
C_{2m}/C_{2e}	0.54	0.46	0.12	0.87
C_{3m}/C_{3e}	1.15	1.75	0.23	2.34
C_{4m}/C_{4e}	0.98	1.07	0.29	0.67
C_{5m}/C_{5e}	1.79	3.31	22.64	1.70
C_{6m}/C_{6e}	2.07	1.26	0.49	1.27
C_{7m}/C_{7e}	0.83	3.85	4.72	0
C_{8m}/C_{8e}	1.61	1.85	0.42	0.73
C_{9m}/C_{9e}	–	6.15	–	

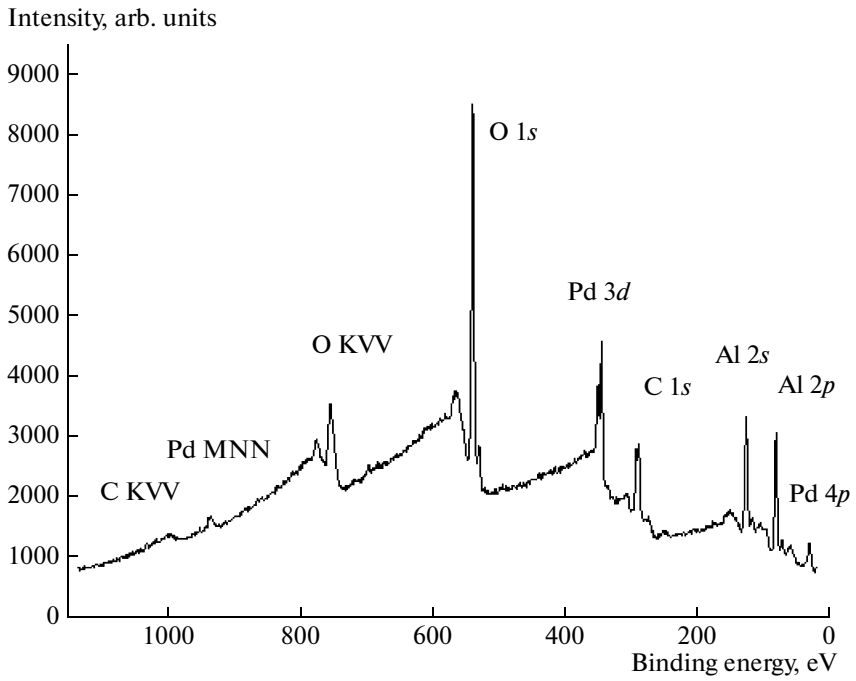

Fig. 5. Survey photoelectron spectrum of Pd–Zn catalyst **III**.

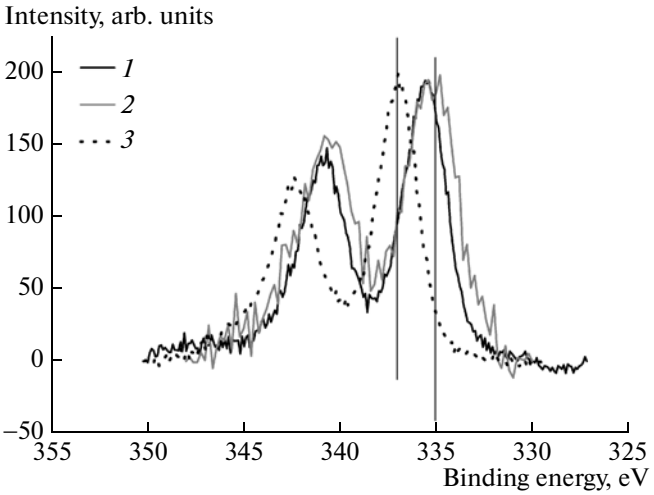

Fig. 6. The Pd 3*d* photoelectron spectra of catalyst **III**: (*1*) a sample after an experiment, (*2*) a reduced sample, and (*3*) an initial sample.

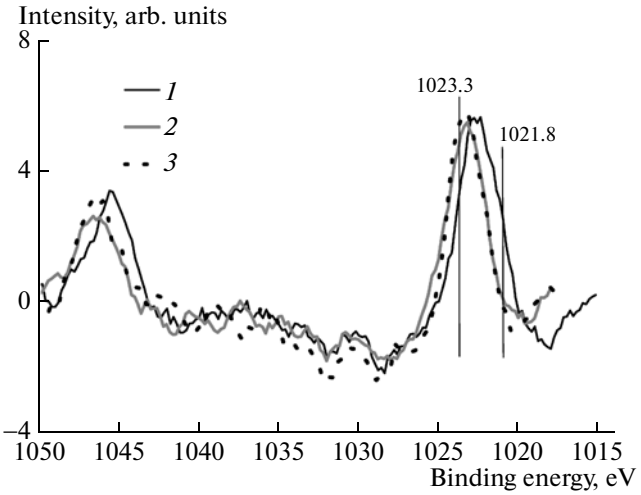

Fig. 7. The Zn 2*p* photoelectron spectra of catalyst **III**: (*1*) a sample after an experiment, (*2*) a reduced sample, and (*3*) an initial sample.

GENESIS OF CATALYTICALLY ACTIVE COMPONENTS UPON SUPPORTING THE PRECURORS AND PRETREATMENT

Study of the States of Active Components by X-ray Photoelectron Spectroscopy

Figure 5 shows a survey spectrum of initial Pd–Zn catalyst **III**. According to quantitative analysis, the surface composition of the catalyst corresponds to the formula $C_{25.1}O_{40.8}Al_{30.5}Pd_3Zn_{0.6}$.

The Pd 3*d* spectrum (Fig. 6) includes data for catalyst **III** in initial and reduced states and after operation. Peaks with binding energies of 337.1 and 335.1 eV correspond to the states Pd^{2+} and Pd^0, respectively. The experimental data indicate that Pd mainly occurred as PdO in the initial catalyst sample, whereas it was partially reduced to palladium metal upon treatment with hydrogen and after an experiment.

Figure 7 shows the spectrum of the Zn 2*p* region for initial, reduced, and spent Pd–Zn catalysts. The

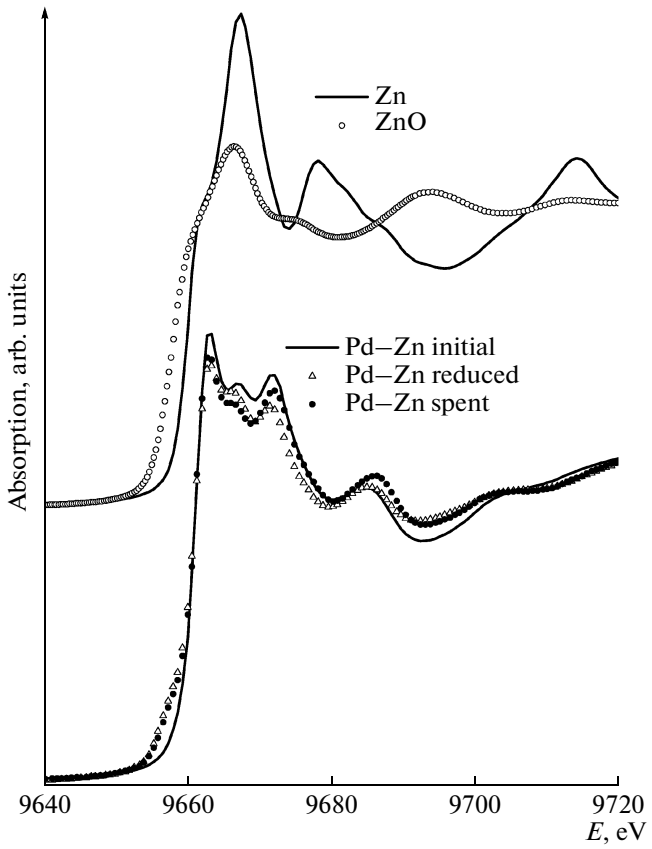

Fig. 8. The *K*-edge XANES spectra of Zn for the samples of Pd–Zn catalyst **III**.

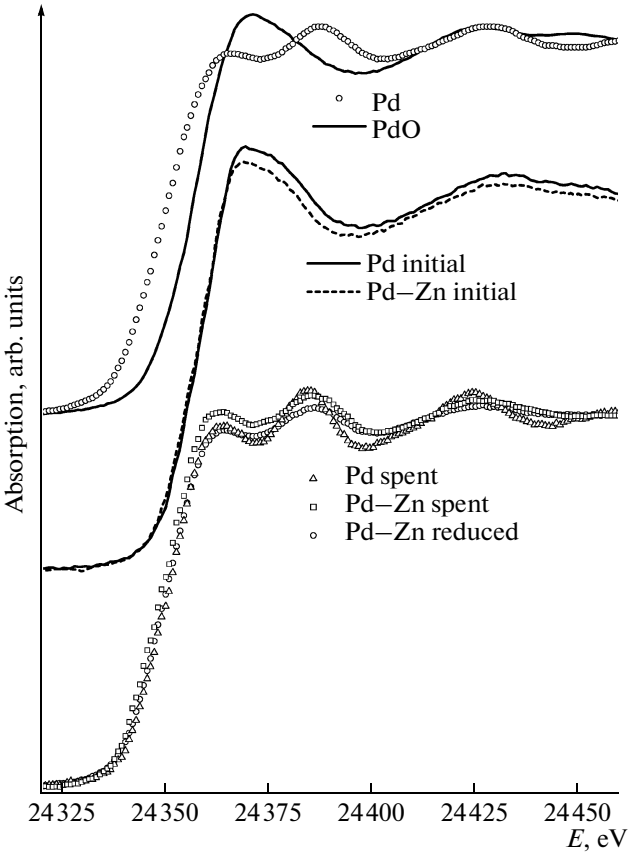

Fig. 9. The *K*-edge XANES spectra of Pd for the samples of Pd–Zn catalyst **III**.

charge states Zn^{2+} and Zn^0 in the spectrum correspond to lines at 1023.3 and 1021.8 eV, respectively. In the experimental spectra, zinc occurred in the state Zn^{2+} (1022.9 and 1022.6 eV); however, a shift of peaks corresponding to the charge state Zn^{2+} allowed us to conclude that, in all of the catalysts, Zn occurred as the oxide $Zn_xAl_{2-x}O_{4\pm\delta}$ with a spinel structure.

Study of the Structure of Active Components by XAFS Spectroscopy

Figures 8 and 9 show the experimental *K*-edge XANES spectra of Zn and Pd. For comparison, data for the reference samples of Pd, PdO, Zn, and ZnO are also given. The *K*-edge position of Zn absorption for freshly prepared catalysts (both pure zinc and zinc–palladium) coincides with that of ZnO; however, the near-edge fine structure is dramatically different (Fig. 8). Therefore, zinc in the catalysts occurs in the oxidized state Zn^{2+} rather than as ZnO. Taking into account published data [17] on a very characteristic XANES spectrum for $ZnAl_2O_4$ with a developed fine structure, we can hypothesize that the major portion of zinc ions diffused into γ-alumina grains to form a near-surface nanocrystalline phase identical to $ZnAl_2O_4$ with Zn in the tetrahedral positions of the spinel structure.

The reductive treatment of the Pd–Zn catalyst with hydrogen at 450°C for 10 h resulted in insignificant changes in the *K*-edge absorption spectrum of Zn: an inflection appeared in the low-energy slope of the line, which is characteristic of Zn^0. In this case, the fraction of zero-valent zinc was no higher than 30%. Analogous changes in XANES spectra were observed for a bimetallic catalyst after a catalytic cycle. In this case, the fraction of reduced Zn was somewhat lower (~20%).

An analysis of the *K*-edge XANES spectra of Pd (Fig. 9) suggests that the state of palladium in the initial catalysts (both mono- and bimetallic) was close to Pd^{2+}. After reductive treatment or catalysis, the absorption spectrum underwent considerable changes to approach the XANES spectrum characteristic of Pd metal.

Figures 10 and 11 show atomic radial distribution (ARD) curves for Zn and Pd, which were obtained by the Fourier transform of experimental EXAFS spectra. Reference curves for Pd, PdO, Zn, and ZnO and the results of the optimization of structural models are also given. Tables 9 and 10 summarize the local environment parameters of Pd and Zn atoms. The experi-

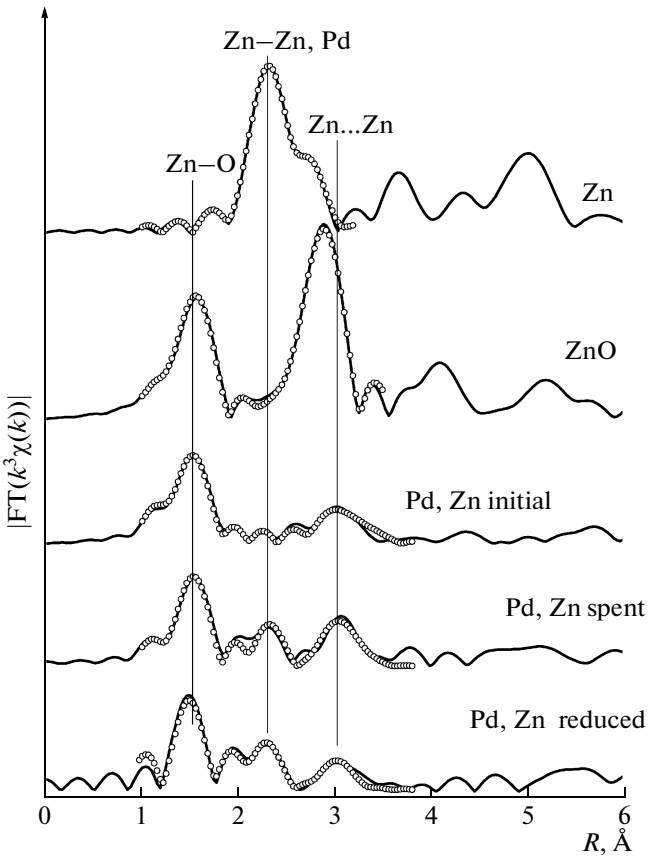

Fig. 10. ARD curves for the local environment of Zn in Pd–Zn catalyst **III** (solid lines) and the results of the refinement of structural models (points).

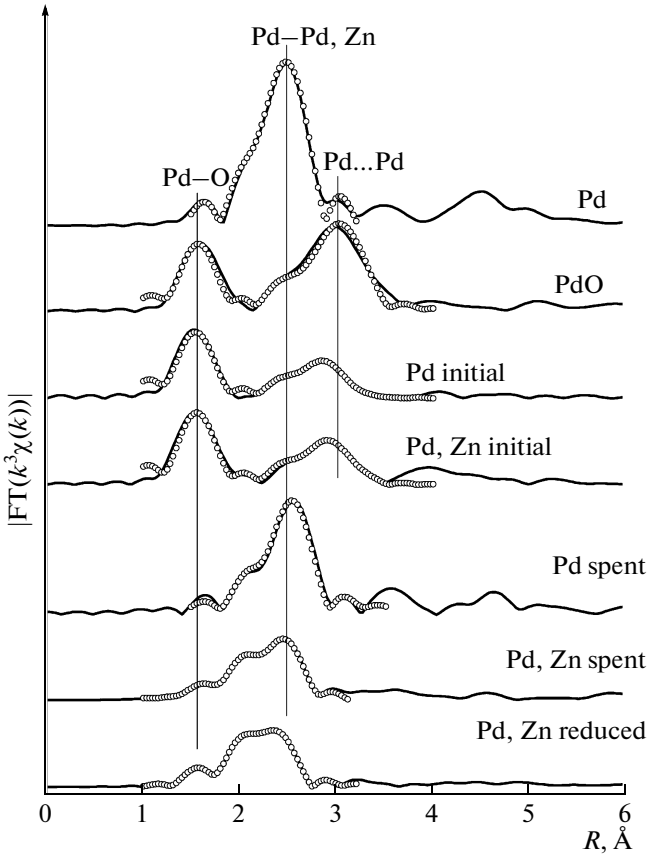

Fig. 11. ARD curves for the local environment of Pd in Pd (**I**) and Pd–Zn (**III**) catalysts (solid lines) and the results of the refinement of structural models (points).

mental results support the above hypothesis that Zn in the Pd–Zn catalyst occurs as a spinel structure because a peak due to the second coordination sphere was observed, and this peak did not coincide with the peak of zinc in ZnO. The ARD curves of reduced samples exhibited a clearly pronounced maximum, which corresponded to a metal–metal bond; this fact suggests the partial formation of a zinc metal phase or the formation of an alloy of Pd and Zn.

As judged from the ARD curve, the local environment of palladium in the initial catalysts is close to PdO. This suggests that palladium atoms form a nanodispersed oxide phase on the support surface.

After treating with hydrogen or performing a catalytic cycle, palladium was almost completely reduced to a metal state, as supported by the disappearance of a peak due to Pd–O in the ARD curve and the appearance of a peak due to Pd–Pd(Zn). Differences in the position and shape of the latter peak for monometallic palladium and bimetallic zinc–palladium catalysts suggest the possible formation of an alloy. This hypothesis was supported by a more detailed simulation of the local environment of palladium atoms (Table 9). In the case of a spent monometallic catalyst, the local environment of Pd consists of palladium atoms. The Pd–Pd distance is 2.80 Å, which is somewhat greater than that in bulk palladium. This increase in the Pd–Pd bond length can be due to hydride formation [18]. On the contrary, a considerable shortening of Pd–Pd bonds was observed in the case of reduced palladium–zinc catalysts. Moreover, Pd–Zn bonds (2.56–2.58 Å) should be involved into the structural model in order to obtain data consistent with experimental results; this is direct evidence for the formation of an intermetallide. Note that the formation of palladium–zinc alloy nanoparticles with similar local structure parameters was observed previously as a result of the reductive treatment of double palladium–zinc carboxylate [19].

Study of the Structure of Active Components by X-ray Diffraction Analysis

Figure 12 shows XRD data for heterometallic system **III** in an initial state and after reduction and catalysis. Note that diffraction data are difficult to interpret because of the occurrence of broad peaks from the initial γ-Al_2O_3 matrix.

As can be seen in Fig. 12, the spectra of the initial Pd–Zn-containing catalytic system exhibited reflec-

Table 9. Local structure parameters obtained by simulating the *K*-edge EXAFS spectra of Zn: coordination number (*N*), interatomic distance (*R*), and Debye–Waller factor (σ^2)

Sample	Coordination sphere	*N*	*R*, Å	σ^2, Å^2
Zn	Zn–Zn	6.0	2.67	0.0065
	Zn–Zn	6.0	2.90	0.0104
ZnO	Zn–O	4.0	1.96	0.0046
	Zn...Zn	6.0	3.16	0.0050
	Zn...Zn	6.0	3.27	0.0050
Pd–Zn initial	Zn–O	3.9	1.94	0.0079
	Zn...Zn	4.2	3.45	0.0110
Pd–Zn spent	Zn–O	2.8	1.92	0.0041
	Zn–Pd	0.8	2.57	0.0060
	Zn...Zn	3.4	3.42	0.0085
Pd–Zn reduced	Zn–O	2.7	1.90	0.0045
	Zn–Zn	0.6	2.46	0.0112
	Zn–Pd	0.8	2.54	0.0043
	Zn...Zn	2.5	3.41	0.0095

Table 10. Local structure parameters obtained by simulating the *K*-edge EXAFS spectra of Pd: coordination number (*N*), interatomic distance (*R*), and Debye–Waller factor (σ^2)

Sample	Coordination sphere	N	*R*, Å	σ^2, Å^2
Pd	Pd–Pd	12	2.74	0.0067
PdO	Pd–O	4.0	2.02	0.0017
	Pd...Pd	4.0	3.03	0.0050
	Pd...Pd	8.0	3.42	0.0050
Pd initial	Pd–O	3.9	2.00	0.0026
	Pd...Pd	2.5	3.02	0.0050
	Pd...Pd	1.7	3.40	0.0050
Pd spent	Pd–Pd	8.9	2.80	0.0067
Pd–Zn initial	Pd–O	4.2	2.01	0.0017
	Pd...Pd	2.6	3.04	0.0050
	Pd...Pd	2.5	3.41	0.0050
Pd–Zn spent	Pd–O	1.3	2.05	0.0124
	Pd–Zn	2.0	2.58	0.0056
	Pd–Pd	8.2	2.72	0.0124
Pd–Zn reduced	Pd–O	0.4	1.99	0.0003
	Pd–Zn	3.4	2.56	0.0091
	Pd–Pd	4.9	2.68	0.0087

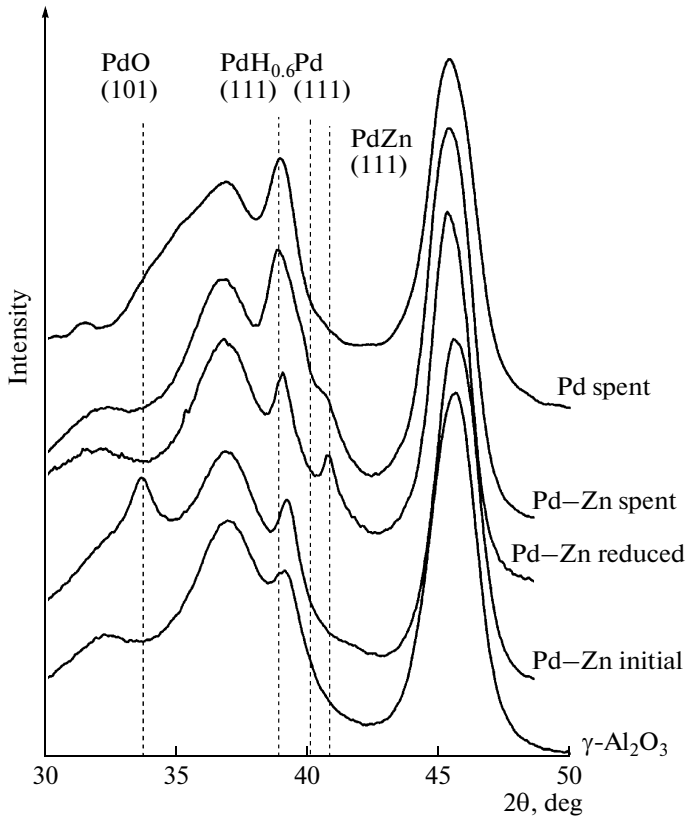

Fig. 12. X-ray diffraction data for γ-Al_2O_3, Pd (**I**), and Pd–Zn (**III**) catalysts. The Pd catalyst was prepared from a palladium acetate complex (for comparison with published data, the angle scale was converted to the Cu$K_{\alpha 1}$ wavelength $\lambda = 1.5406$ Å).

tions characteristic of a PdO phase [20]. After the step of reduction, the diffraction pattern of the catalyst sample exhibited no peaks due to the PdO phase and peaks characteristic of the palladium hydride $PdH_{0.6}$ [21] and a Pd–Zn alloy (1 : 1) [22] appeared. Consequently, in the course of hydrogen treatment at 450°C, Pd(II) was reduced to Pd(0). In this case, the phases of palladium hydride and an alloy with zinc were formed. After a catalytic experiment with the Pd–Zn catalyst, a decrease in the peak intensity corresponding to the Pd–Zn alloy and an increase in the intensity of a peak due to $PdH_{0.6}$ were observed. In this case, we can state the occurrence of reflections corresponding to a Pd metal phase [23]. The analogous formation of a hydride phase was also observed in the monometallic Pd catalyst, as demonstrated by EXAFS data.

The decrease in the intensity of a peak corresponding to a Pd–Zn alloy after catalysis suggests that alloy particles can be active sites in the test reaction. Previously, the high selectivity of catalysts based on Pd–Zn alloys in the steam conversion reaction of methanol was demonstrated [24–26].

Based on the experimental structural data, we can conclude that the phase composition of active components essentially depends on pretreatment conditions (Table 11).

Table 11. Phase composition of active components at the stages of catalyst pretreatment

No.	Brief notation	Phase composition after pretreatment	
		stage 1	stage 2
I	Pd	PdO	[$PdH_{0.6}$ + Pd]
II	Zn	$Zn_xAl_2O_{3+x\pm\delta}$	$Zn_xAl_2O_{3+x\pm\delta}$
III	Pd–Zn	PdO + $Zn_xAl_2O_{3+x\pm\delta}$	[$PdH_{0.6}$ + Pd + PdZn] + $Zn_xAl_2O_{3+x\pm\delta}$
IV	Pd + Zn	PdO + $Zn_xAl_2O_{3+x\pm\delta}$	[$PdH_{0.6}$ + Pd] + $Zn_xAl_2O_{3+x\pm\delta}$
V	Pd/Zn	[$PdH_{0.6}$ + PdZn]	[$PdH_{0.6}$ + PdZn]

The evolution scheme of phase transformations of active components at all stages of preparation and catalysis for a bimetallic catalyst, which exhibited the highest activity, is given below:

$$\mathrm{Pd(II)Zn(II)(OAc)_4(OH)_2/Al_2O_3} \xrightarrow{\text{Ar, 500°C}} \mathrm{PdO} + \mathrm{Zn_xAl_2O_{3+x\pm\delta}} \xrightarrow{\mathrm{H_2}\text{, 450°C}} [\mathrm{PdH_{0.6}} + \mathrm{PdZn}] + \mathrm{Zn_xAl_2O_{3+x\pm\delta}} \xrightarrow{\text{catalysis}} [\mathrm{PdH_{0.6}} + \mathrm{Pd} + \mathrm{PdZn}] + \mathrm{Zn_xAl_2O_{3+x\pm\delta}}.$$

From the above scheme, it follows that metal and oxide clusters are formed on the support surface in the course of the preparation of a Pd–Zn-containing catalyst; these clusters can possess hydrogenating and condensing functions.

CONCLUSIONS

The supporting of the bimetallic complex $Pd(\mu\text{-}OOC\text{-}Me)_4Zn(OH_2)$ and the monometallic acetate complexes $Zn(OAc)_2 \cdot 2H_2O$ and $Pd_3(OAc)_6$ onto the surface of $\gamma\text{-}Al_2O_3$ followed by thermal treatment and reductive activation results in the formation of two types of active components: (1) a hydrogenating component as the clusters of Pd metal, Pd hydride, and Pd_xZn_y alloy and (2) oxide components as the mixed zinc–aluminum spinel $Zn_xAl_{2-x}O_{4\pm\delta}$. The results of the study on the catalytic activity of the resulting systems in the reactions of ethanol conversion demonstrated that the active components formed from a bimetallic precursor exert a complementary effect to increase the total yield of hydrocarbons by 10–15%. At the same time, the selectivity for alkane and alkene formation directly depends on the composition of the catalytic system. The Pd-containing catalyst exhibited an enhanced activity in the reductive dehydration of ethanol to gasoline-fraction alkanes, primarily, of linear structure, in accordance with overall reaction scheme (I). The Zn-containing system with the spinel structure exhibits selectivity for the condensation of ethanol carbon skeleton into alkenes of the above fraction, but containing to 50% branched-chain hydrocarbons according to reaction (II). The complementary effect of active components, which results in an increase in the formation of a C_3–C_{10} alkane–alkene fraction in the reaction occurs in the presence of palladium metal clusters and complex zinc–aluminum oxide distributed over the surface of $\gamma\text{-}Al_2O_3$, probably, at a short distance from each other.

The reductive dehydration reaction of ethanol occurs with the release of large amounts of methane, ethane, and carbon monoxide, which are formed by ethylene hydrogenation reaction and reactions (IV) and (V), to cause a decrease in the total yield of the target C_4–C_{10} fraction. It is most likely that the formation of carbon dioxide was due to the water gas shift reaction. The conversion of ethanol by reaction (II) with the formation of alkenes is characterized by a higher yield of aliphatic hydrocarbons, which is as high as 40–50 wt % on a starting ethanol basis, and a considerable amount of branched-chain structures (to 50 wt %).

These conclusions were supported by selectivity changes depending on the phase composition of the catalyst formed upon various catalyst pretreatment procedures. In the case of a long reductive treatment with H_2, a higher concentration of the Pd–Zn alloy and a lower concentration of oxide with the structure of a complex spinel are formed on the surface of alumina. In this case, a more considerable contribution of the reductive dehydration of ethanol is observed, which leads to the formation of linear alkanes. Upon the formation of a catalytic system by thermal treatment in Ar followed by reduction in H_2, to 80% zinc atoms on the surface of alumina are incorporated into the structure of a complex oxide; the remaining zinc atoms enter into the composition of Pd_xZn_y intermetallide clusters. Palladium metal clusters are also formed on the support surface. In this case, the yield of the hydrocarbon fraction increases because of reaction (II), which leads to the formation of branched-chain olefins. In this case, the yield of C_1–C_2 light alkanes and carbon oxides considerably decreases.

In general, it is believed that the bifunctional mechanism of alcohol conversion consists in the condensation reaction of a carbon skeleton, which occurs at acid sites, followed by hydrogen transfer to olefins on the resulting clusters of palladium hydride.

It is most likely that, upon the preparation of a catalyst from a heterometallic precursor, an optimum ratio between closely spaced metal and oxide sites is formed on the support surface after thermal treatment followed by reduction. As a result of more closely spaced hydrogenating and condensing active sites, the spillover of hydrogen to unsaturated alkenes chemisorbed on the surface is facilitated and, correspondingly, a smaller amount of hydrogen is consumed for the deep hydrogenation of ethanol to methane.

Thus, we demonstrated for the first time that the selectivity of ethanol conversion can be controlled by changing catalyst composition. This makes it possible to obtain aliphatic hydrocarbon fractions with alkane concentrations higher than 90 wt %, aliphatic hydrocarbon fractions with alkene concentrations to 70 wt %, and an alkane–olefin fraction.

The addition of glycerol to ethanol mainly results in an increase in the yield of alkenes, and it decreases the possibility of affecting the composition of reaction products upon changes in the catalyst composition. However, glycerol is an active coreactant, which participates in hydrocarbon chain growth according to reaction (III); it leads to a decrease in the yields of methane and ethane and an increase in the yield of the target fraction of aliphatic hydrocarbons to 55 wt %, that is, more than 80% on a theoretical basis.

REFERENCES

1. Tsodikov, M.V., Kugel, V.Ya., Slivinskii, E.V., Zaikin, V.G., Mordovin, V.P., Colon, G., Hidalgo, M.C., and Navio, J.A., *Langmuir*, 1999, vol. 15, p. 6601.
2. Tsodikov, M.V., Kugel, V.V., Yandieva, F.A., Mordovin, V.P., Gekhman, A.E., and Moiseev, I.I., *Pure Appl. Chem.*, 2004, vol. 76, no. 9, p. 1769.
3. Tsodikov, M.V., Kugel', V.Ya., Yandieva, F.A., Kliger, G.A., Glebov, L.S., Mikaya, A.I., Zaikin, V.G., Slivinskii, E.V., Plate, N.A., Gekhman, A.E., and Moiseev, I.I., *Kinet. Katal.*, 2004, vol. 45, no. 6, p. 904 [*Kinet. Catal.* (Engl. Transl.), vol. 45, no. 6, p. 854].
4. RF Patent 2391133, 2010.
5. Tsodikov, M.V., Yandieva, F.A., Kugel, V.Ya., Chistyakov, A.V., Gekhman, A.E., and Moiseev, I.I., *Catal. Lett.*, 2008, vol. 121, nos. 3-4, p. 199.
6. Tsodikov, M.V., *Tezisy III Rossiiskoi konf. "Aktual'nye problemy neftekhimii"* (Proc. III Russian Conf. on Current Topics in Petroleum Chemistry), Zvenigorod, Moscow oblast, 2009, p. 156.
7. Ichikawa, J.M., *Catal. Lett.*, 1979, vol. 59, p. 127.
8. Maksimov, Yu.V., Matveev, V.V., Suzdalev, I.P., Slinkin, A.A., Fedorovskaya, E.A., Kutyreva, N.A., Khomenko, T.I., and Kadushin, A.A., *Kinet. Katal.*, 1989, vol. 30, p. 1198.
9. Tkachenko, O.P., Stakheev, A.Yu., Kustov, L.M., Mashkovsky, M., Berg, GrunertW., Kozitsyna, N.Yu., Nefedov, S.E., Dobrokhotova, Zh.V., Shilov, V.I., Vargaftik, M.N., and Moiseev, I.I., *Catal. Letters*, 2006, vol. 112, p. 155.
10. Mashkovsky, I.S., Tkachenko, O.P., Stakheev, A.Yu., Kozitsyna, N.Yu., Nefedov, S.E., Vargaftik, M.N., Cano, F.M., and Molenbroek, A.M., *Proc. 13th Nordic Symp. on Catalysis*, Göteborg, 2008, p. 194.
11. Kozitsyna, N.Yu., Nefedov, S.E., Dolgushin, F.M., Cherkashina, N.V., and Vargaftik, M.N., Moiseev. I.I., *Inorg. Chim. Acta*, 2006, vol. 359, p. 2072.
12. Chernyshov, A.A., Veligzhanin, A.A., and Zubavichus, Y.V., *Nucl. Instrum. Methods Phys. Res., Sect. A*, 2009, p. 95.
13. Ravel, B. and Newville, M., *J. Synchrotron Radiat.*, 2005, vol. 12, p. 537.
14. Ankudinov, A.L., Ravel, B., Rehr, J.J., and Conradson, S.D., *Phys. Rev. B: Condens. Matter*, 1998, vol. 58, p. 7565.
15. Yandieva, F.A., Tsodikov, M.V., Chistyakov, A.V., Kugel', V.Ya., Zubavichus, Ya.V., Veligzhanov, A.A., Kitaev, L.E., Yushchenko, V.V., Gekhman, A.E., and Moiseev, I.I., *Kinet. Katal.*, 2010, vol. 51, no. 4, p. 572 [*Kinet. Catal.* (Engl. Transl.), vol. 51, no. 4, p. 548].
16. Tsodikov, M.V., Chistyakov, A.V., Yandieva, F.A., Gekhman, A.E., and Moiseev, I.I., *Second German–Russian Seminar on Catalysis*, Munich, 2010, p. 22.
17. Revel, R., Bazin, D., Elkaim, E., Kihn, Y., and Dexpert, H., *J. Phys. Chem. B*, 2000, vol. 104, p. 9828.
18. Davis, R.J., Landry, S.M., Horsley, J.A., and Boudart, M., *Phys. Rev. B: Condens. Matter*, 1989, vol. 39, p. 10 580.
19. Kozitsyna, N.Yu., Nefedov, S.E., Dobrokhotova, Zh., Ikorskii, V.N., Stolyarov, I.P., Vargaftik, M.N., and Moiseev, I.I., *Ross. Nanotekhnol.*, 2008, no. 3, p. 100.
20. Waser, J., Levy, H.A., and Peterson, S.W., *Acta Crystallogr.*, 1953, no. 6, p. 661.
21. Khodyrev, Yu.P., Baranova, R.V., Imamov, R.M., and Semiletov, S.A., *Izv. Akad. Nauk SSSR, Neorg. Mater.*, 1978, no. 14, p. 1645.
22. Nowotny, H. and Bittner, H., *Monatsh. Chem.*, 1950, no. 81, p. 679.
23. Hull, A.W., *Phys. Rev.*, 1921, vol. 17, p. 571.
24. Neyman, K.M., Lim, K.H., Chen, Z.-X., Moskaleva, L.V., Bayer, A., Reindl, A., Borgmann, D., Denecke, R., Steinruck, H.-P., and Rosch, N., *Phys. Chem. Chem. Phys.*, 2007, no. 9, p. 3470.
25. Iwasa, N., Mayanagi, T., Masuda, S., and Takezawa, N., *React. Kinet. Catal. Lett.,* 2000, vol. 69, no. 2, p. 350.
26. Fukuhara, C., Kamata, Y., and Igarashi, A., *Appl. Catal., A*, 2007, vol. 330, p. 108.